

Multiferroic $\text{Bi}_2\text{NiMnO}_6$ Thin Films: A Computational Prediction

Oswaldo Diéguez^{1,2} and Jorge Íñiguez³

¹*Department of Materials Science and Engineering,
Faculty of Engineering, Tel Aviv University,
Tel Aviv 69978, Israel*

²*The Raymond and Beverly Sackler Center for Computational Molecular and Materials Science,
Tel Aviv University, Tel Aviv 69978, Israel*

³*Materials Research and Technology Department,
Luxembourg Institute of Science and Technology,
5 avenue des Hauts-Fourneaux,
L-4362 Esch/Alzette, Luxembourg*

(Dated: November 12, 2018)

We report first-principles calculations for one of the few materials that is believed to be a ferroelectric ferromagnet, $\text{Bi}_2\text{NiMnO}_6$. Our calculations show that, contrary to what it has been reported so far, bulk $\text{Bi}_2\text{NiMnO}_6$ does not have a polarization. Instead, like BiMnO_3 , it crystallizes into a centrosymmetric structure with space group $C2/c$. We also predict that $\text{Bi}_2\text{NiMnO}_6$ will indeed be a ferroelectric ferromagnet if it is grown as an epitaxial film on a substrate with in-plane square symmetry and a lattice constant around 4 Å, such as BaTiO_3 or $\text{PbZr}_{1-x}\text{Ti}_x\text{O}_3$.

PACS numbers: 77.84.-s, 75.85.+t, 71.15.Mb

I. INTRODUCTION

The possibility of manipulating the magnetization of a material by using an electric field is probably the most attractive envisioned application of magnetoelectric multiferroics—ferroelectrics with magnetic ordering.¹ Even if the mechanisms responsible for ferroelectricity and magnetism are somewhat exclusive of each other,^{2,3} in the last decade a large research effort has gone into searching for these materials.^{4–16} This effort has mainly focused on two groups of complex oxides: those where different species are responsible for the polarization and the magnetism, and those where the magnetic ordering breaks the inversion symmetry of the structure to create a small polarization. BiFeO_3 belongs to the first group and it is by far the most studied multiferroic,¹⁷ mainly because it keeps both its ferroic orderings well above room temperature; it is also relatively easy to prepare in bulk and film form, and it has a simple crystal structure—a perovskite where inversion symmetry is broken to accommodate the lone pair of Bi in the A site, while the B site harbors the Fe ions whose d electrons are responsible for magnetism. However, the ferromagnetic component in BiFeO_3 is tiny; instead, the spins of two neighboring Fe ions are almost perfectly antiparallel. In the difficult search for single-phase ferroelectric ferromagnets that would allow for a direct hysteresis loop of magnetization with electric field some candidate materials have been proposed. Examples include EuTiO_3 (although ferromagnetism only settles at around 4 K¹⁸), LuFe_2O_4 (although whether this is a ferroelectric is still under debate^{19,20}), Fe_3O_4 (although the exact

structure that arises below the Verwey transitions is not yet understood²¹), CoCr_2O_4 (although both the magnetization and the polarization are very small²²), and, more recently, the metastable $\epsilon\text{-Fe}_2\text{O}_3$.²³

Researchers have also explored perovskite oxides similar to BiFeO_3 , but with other transition-metal ions instead of Fe. BiMnO_3 is the only member of this group that displays strong ferromagnetism. Initial reports attributed a polar $C2$ space group to bulk BiMnO_3 ,^{24,25} but more recent studies agree in that this is a paraelectric with $C2/c$ symmetry.^{26–28} It is possible to change the structure of this material by growing it as an epitaxial thin film, although the calculations of Spaldin and Hatt²⁹ showed that when the substrate-imposed distortion is small enough to keep the ferromagnetism in BiMnO_3 , then a polarization does not develop, and our calculations³⁰ showed that when the distortion is large enough to create a large polarization, then ferromagnetism turns into antiferromagnetism. Another way to try to modify the properties of these oxides is to add a second species in one of the sites of the perovskite. Azuma and coworkers reasoned that the Goodenough-Kanamori rules^{31,32} predict a ferromagnet if Mn and Ni shared the sites inside O_6 octahedra in a rock-salt pattern; when they prepared $\text{Bi}_2\text{NiMnO}_6$ by high-pressure synthesis, they indeed measured large parallel magnetic moments,³³ which persisted up to a Curie temperature of 140 K. After their synchrotron X-ray powder diffraction, they concluded that the material shows a heavily distorted double perovskite structure where the Ni^{2+} and Mn^{4+} ions are indeed ordered in a rock-salt configuration; they assigned the space group $C2$ to this crystal. Later, first-principles calculations characterized further

this structure and quoted a value of the polarization around $20 \mu\text{C}/\text{cm}^2$.^{34–36}

Unlike those previous studies, our first-principles calculations show that bulk $\text{Bi}_2\text{NiMnO}_6$ is actually a paraelectric material with $C2/c$ space group, the same situation as with BiMnO_3 . However, we predict that when $\text{Bi}_2\text{NiMnO}_6$ films are grown under achievable tensile epitaxial strain, it will indeed become a ferroelectric ferromagnet with a large polarization ($70 \mu\text{C}/\text{cm}^2$) and a magnetization above $2 \mu_B$ per transition metal cation, as in the bulk compound.³³ We describe the methodology we have used for our calculations in Section II, present our results for the bulk material in Section III.A and for epitaxial films in Section III.B, and summarize the implications of our work in Section IV.

II. METHODS

Our first-principles calculations are based on density-functional theory (DFT).^{37,38} Following our previous study of BiMnO_3 ,³⁰ we used two methods to treat the localized d orbitals of Ni^{2+} and Mn^{4+} : (i) DFT with a ‘‘Hubbard U ’’,³⁹ using $U_{\text{Ni}} = 1 \text{ eV}$, $J_{\text{Ni}} = 0 \text{ eV}$, $U_{\text{Mn}} = 4 \text{ eV}$, and $J_{\text{Mn}} = 1 \text{ eV}$; and (ii) DFT with the HSE06 hybrid functional.⁴⁰ For all our calculations we have used the VASP⁴¹ code; for this system, the second method demands two orders of magnitude more computer time than the first, but it predicts band gaps for solids that are much closer to experimental results,⁴⁰ and in particular it performs well for perovskite oxides such as BiFeO_3 .⁴²

We used the Perdew-Burke-Ernzerhof DFT exchange-correlation functional adapted to solids (PBEsol).⁴³ To treat the ionic cores we resorted to the projector augmented-wave method,⁴⁴ solving for the following electrons: Ni’s and Mn’s $3p$, $3d$, and $4s$; Bi’s $5d$, $6s$, and $6p$; and O’s $2s$ and $2p$. The plane-wave basis set kinetic-energy cutoff was 500 eV . We performed integrations in the Brillouin zone using k -point grids with densities similar to that of the $6 \times 6 \times 6$ mesh for a 5-atom perovskite unit cell.

III. RESULTS

A. Bulk Phases

Our first set of calculations involves the optimization of $\text{Bi}_2\text{NiMnO}_6$ bulk structures that might be competitive in energy with the ground state. As mentioned in the Introduction, previous experimental and computational studies consider that this ground state belongs to the $C2$ space group; Refs. 33 and 34 report the lattice parameters and Wickoff positions of the atoms in the crystal unit cell, and we have run optimizations starting from those configurations. In the future we call this structure GS—the

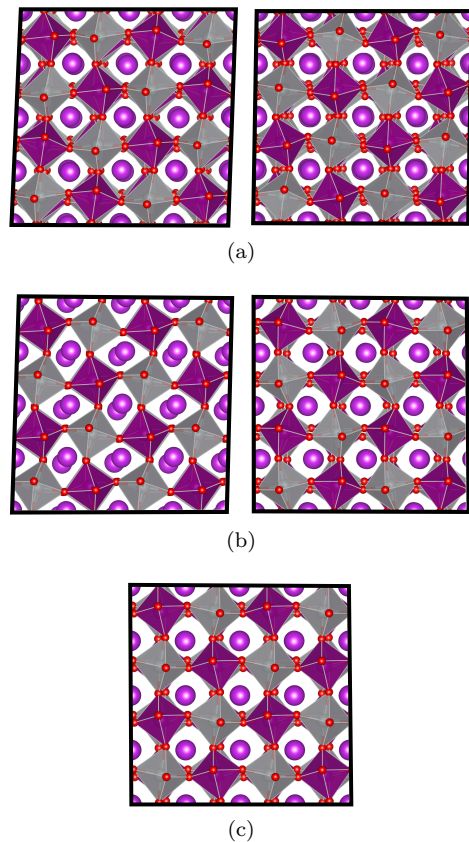


FIG. 1. (Color online.) Inequivalent side views of a pseudocubic unit cell for bulk $\text{Bi}_2\text{NiMnO}_6$ structures that correspond to energy minima according to our DFT+ U calculations: (a) $C2/c$, (b) $P2_1/n$, and (c) $R3$.

structure that the bulk material displays at low temperature and low pressure. Another relevant phase is the one observed at high temperature with space group $P2_1/n$, fully described in Ref. 45; this phase is analogous to the $Pnma$ phase that appears in many BiMO_3 perovskites at high pressure and/or high temperature,⁴⁶ but with reduced symmetry because of the superimposed rock-salt pattern of Ni^{+2} and Mn^{+4} cations. By analogy with our previous paper about BiMnO_3 ,³⁰ we call this paraelectric phase p . Based on our previous experience in the search of new phases of BiFeO_3 ,⁴⁷ BiCoO_3 ,⁴⁸ and BiMnO_3 ,³⁰ we also relaxed ferroelectric phases similar to the rhombohedral ground state of BiFeO_3 (so-called R phases) and to the supertetragonal ground state of BiCoO_3 (so-called T phases); we have enforced the same rock-salt cation pattern known to exist in both experimentally characterized phases of $\text{Bi}_2\text{NiMnO}_6$. We have optimized these structures using the DFT+ U and the HSE06 methods, obtaining similar results with both approaches regarding their structural details. The atomic structure of the resulting optimized structures (with forces converged below $0.015 \text{ eV}/\text{\AA}$ and stress components below 0.1 GPa) is shown in Figure 1, while Table I contains the values of several magnitudes of interest for these phases.

TABLE I. Properties of $\text{Bi}_2\text{NiMnO}_6$ phases that are local energy minima according to our calculations (with DFT+ U and HSE06), and comparison with experiment (from Refs. 33 and 45). We report the space group, lattice parameters, lattice angles, Wickoff positions, polarization P , and energy difference with the GS phase ΔE . GS, p , and R label the ground-state phase, the high-temperature paraelectric phase, and the R rhombohedral phase found in this study, respectively.

Phase	Properties	DFT+ U	HSE06	Exp.	
GS	Space group	$C2/c$	$C2/c$	$C2$	
	a (Å)	9.3871	9.3523	9.4646	
	b (Å)	5.3739	5.3558	5.4230	
	c (Å)	9.5355	9.4679	9.5431	
	β ($^\circ$)	107.64	107.66	107.82	
	Mn 1	(0.2500, 0.2500, 0.0000)	(0.2500, 0.2500, 0.0000)	(0.257, 0.250, 0.001)	
	Ni 1	(0.0000, 0.2648, 0.2500)	(0.0000, 0.2609, 0.2500)	(0.000, 0.252, 0.250)	
	Ni 2	–	–	(0.000, 0.737, 0.750)	
	Bi 1	(0.6308, 0.2323, 0.1235)	(0.6314, 0.2230, 0.1248)	(0.633, 0.214, 0.128)	
	Bi 2	–	–	(0.631, 0.772, 0.627)	
	O 1	(0.5897, 0.1970, 0.5833)	(0.5914, 0.1949, 0.5823)	(0.611, 0.176, 0.599)	
	O 2	(0.1582, 0.0385, 0.3860)	(0.1602, 0.0344, 0.3860)	(0.146, 0.013, 0.386)	
	O 3	(0.3498, 0.0350, 0.1577)	(0.3493, 0.0374, 0.1565)	(0.333, -0.021 , 0.163)	
	O 4	–	–	(0.920, 0.279, 0.430)	
	O 5	–	–	(0.377, 0.941, 0.649)	
	O 6	–	–	(0.662, 0.453, 0.876)	
	P ($\mu\text{C}/\text{cm}^2$)	0	0	N/A	
	ΔE (meV/f.u.)	0	0	–	
p	Space group	$P2_1/n$	$P2_1/n$	$P2_1/n$	
	a (Å)	5.3590	5.3182	5.4039	
	b (Å)	5.5522	5.5262	5.5668	
	c (Å)	7.6517	7.6007	7.7330	
	β ($^\circ$)	90.00	90.00	90.166	
	Mn 1	(0.0000, 0.5000, 0.0000)	(0.0000, 0.5000, 0.0000)	(0.0000, 0.5000, 0.0000)	
	Ni 1	(0.5000, 0.0000, 0.0000)	(0.5000, 0.0000, 0.0000)	(0.5000, 0.0000, 0.0000)	
	Bi 1	(0.0086, 0.0549, 0.2509)	(0.0072, 0.0553, 0.2512)	(0.0049, 0.0468, 0.2510)	
	O 1	(0.3067, 0.2878, 0.4589)	(0.3109, 0.2860, 0.4589)	(0.280, 0.279, 0.477)	
	O 2	(0.2921, 0.3040, 0.0386)	(0.2907, 0.3080, 0.0380)	(0.281, 0.281, 0.053)	
	O 3	(0.58372 $-$ 0.0222, 0.2556)	(0.5851, -0.0238 , 0.2583)	(0.594, -0.022 , 0.252)	
		P ($\mu\text{C}/\text{cm}^2$)	0	0	0
		ΔE (meV/f.u.)	-30	24	–
	R	Space group	$R3$	$R3$	–
		a (Å)	5.4526	5.4428	–
		α ($^\circ$)	60.35	60.02	–
Mn 1		(0.7250, 0.7250, 0.7250)	(0.7208, 0.7208, 0.7208)	–	
Ni 1		(0.2284, 0.2284, 0.2284)	(0.2255, 0.2255, 0.2255)	–	
Bi 1		(0.0000, 0.0000, 0.0000)	(0.0000, 0.0000, 0.0000)	–	
Bi 2		(0.4985, 0.4985, 0.4985)	(0.4987, 0.4987, 0.4987)	–	
O 1		(0.4114, -0.0566 , 0.5483)	(0.4122, -0.0646 , 0.5450)	–	
O 2		(0.0330, 0.4609, -0.0967)	(0.0225, 0.4580, -0.1000)	–	
		P ($\mu\text{C}/\text{cm}^2$)	70	79	–
		ΔE (meV/f.u.)	-4	17	–

The main results from Table I is that (i) our attempts to optimize the polar $C2$ phase always ended up in a non-polar structure with $C2/c$ space group; (ii) our PBSsol+ U and HSE06 methods give different predictions regarding which phase is the ground state of bulk $\text{Bi}_2\text{NiMnO}_6$; (iii) there is a ferromagnetic R phase with large polarization that is competitive with the phases

known so far to exist, and (iv) no T phase is obtained as a result of our optimizations. In the following, we provide more details about each of these points.

The original assignment of space group $C2$ to the GS phase³³ was done after obtaining synchrotron X-ray powder diffraction peaks that could be indexed as a monoclinic unit cell with the lattice parameters quoted in

Table I. Because the unit cell was similar to that of BiMnO_3 , a Rietveld refinement was performed by assuming an initial model related to that BiMnO_3 structure, and the validity of this model seemed satisfactory. At the time, the space group BiMnO_3 was being described as $C2$, but later it was shown^{26–28} that it is $C2/c$. While $C2/c$ is centrosymmetric, the $C2$ space group allows for a polarization along the monoclinic axis; calculations assuming a point-charge model or using the Berry-phase first-principles theory gave a value of around $20 \mu\text{C}/\text{cm}^2$.^{33–36,49} As far as we know, no experimental measurement of the polarization has been done for bulk $\text{Bi}_2\text{NiMnO}_6$.

Our attempts to find a metastable $C2$ phase for $\text{Bi}_2\text{NiMnO}_6$ failed. Every structure we have set with that space group lowered its energy when their atoms were allowed to move, ending always in the $C2/c$ structure displayed in Fig. 1(a). This also happens for BiMnO_3 : different $C2$ structures converge to the same lower-energy $C2/c$ structure.^{28,30} We must however mention that previous first-principles calculations³⁴ did report that a $C2$ phase was found after optimization (albeit with quite different Wickoff positions than the experimental work). We have tried to reproduce those calculations using a methodology similar to that of Ref. 34, but by allowing enough relaxation steps the optimized structure slowly converged to the $C2/c$ one presented here. Other first-principles studies of $\text{Bi}_2\text{MnNiO}_6$ were done either fixing the structure to the experimental one^{35,49} or to the relaxed first-principles one of Ciucivara and coworkers.³⁶ Further support for the $C2/c$ space group is that the reported $C2$ structure contains two different environments for the Ni^{2+} ions and one for the Mn^{4+} ions, but there is no explanation so far for this—there are no signs of charge or orbital ordering, for example.

To add to the puzzle of the possible paraelectricity of bulk $\text{Bi}_2\text{NiMnO}_6$, a sizable polarization has indeed been measured in $\text{Bi}_2\text{NiMnO}_6$ *films*. The group that synthesized this double perovskite for the first time in bulk also grew it as a film on SrTiO_3 using pulsed laser deposition.⁵⁰ They measured a polarization of $5 \mu\text{C}/\text{cm}^2$ and a magnetic Curie temperature of 100 K. Their films displayed a pseudotetragonal structure with $a = b = 3.91 \text{ \AA}$ (matching the substrate) and $c = 3.87 \text{ \AA}$, described as rather different from the bulk one, while keeping the same rock-salt pattern.⁵¹ Using a chemical solution deposition method, Lai *et al.*⁵² grew $\text{Bi}_2\text{NiMnO}_6$ films with and without SrTiO_3 buffer layers on a $\text{Pt}(111)/\text{Ti}/\text{SiO}_2/\text{Si}(100)$ substrate, obtaining polarizations around 6 and $8 \mu\text{C}/\text{cm}^2$. Again, the situation can be compared to that of BiMnO_3 , where polarizations between 9 and $23 \mu\text{C}/\text{cm}^2$ have been reported for films,^{53–55} even if the bulk is nonpolar. For BiMnO_3 we proposed that those measurements might be related to the formation of film phases under strain that are polar.³⁰

We move on now to the issue of the predicted ground state by different methodologies. Table I shows that the three local minima of the energy surface of $\text{Bi}_2\text{NiMnO}_6$

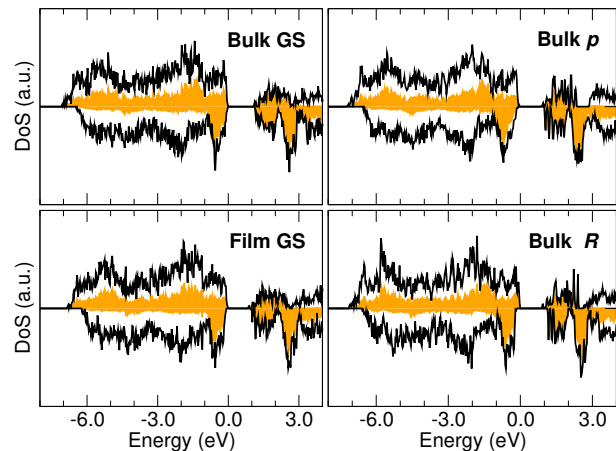


FIG. 2. (Color online.) DFT+ U density of states for the three bulk phases that are local minima of the energy, and for the GS epitaxial film at in-plane lattice parameter of 4 \AA . The lines represent the total density of states, and the shaded areas correspond to its projection onto the d orbitals of Ni and Mn (hybridized mostly with the p orbitals of O).

lie within only 30 meV per formula unit (five-atom group of the standard perovskite unit cell; in our case, $\text{BiNi}_{1/2}\text{Mn}_{1/2}\text{O}_3$). Our DFT+ U method predicts a higher energy for the GS phase than for the other two; this happened too for BiMnO_3 ,³⁰ where the situation is corrected by the HSE06 hybrid. We have shown in the past that different exchange-correlation functionals predict almost the same minima of the energy surface of BiMnO_3 ³⁰ and BiFeO_3 ,⁴⁷ although how those minima are ordered in energy can vary from functional to functional. As for BiMnO_3 , here we use the fast DFT+ U method when we are interested in finding possible energy minima, or when we are interested in energy differences between very similar structures, while we will resort to the more accurate and slow HSE06 when it is important to evaluate energy differences between different phases.

Both DFT+ U and HSE06 predict that there exists a metastable ferromagnetic rhombohedral structure with a polarization around $70 \mu\text{C}/\text{cm}^2$ when computed using the Berry-phase formalism (we have checked that typical antiferromagnetic alignments are higher in energy; details are given later for similar films). This is a structure like that of bulk BiFeO_3 , but where the superimposed rock-salt pattern of Mn^{4+} and Ni^{2+} causes a reduction from the $R3c$ space group to the $R3$ symmetry; it is represented in Fig. 1(c). According to first principles calculations, a similar structure is also metastable for BiCoO_3 ⁴⁸ and BiMnO_3 .³⁰

Regarding the electronic structure, the GS, p , and R phases display similar density of states profiles, as shown in Fig. 2 (this was also the case for different phases in BiFeO_3 ⁴⁷). The band gap in all cases is around 1 eV.

Unlike in BiCoO_3 , BiFeO_3 , and BiMnO_3 , no T structures appeared as local minima of the energy in our $\text{Bi}_2\text{NiMnO}_6$ search. We relaxed variations of the T con-

figurations of those other materials with the added rock-salt pattern of Mn^{4+} and Ni^{2+} , but the resulting structure was always one of the other three local minima.

B. Epitaxial Films

One possible way to stabilize a metastable phase of the bulk of a material is to grow it as a thin film on a substrate; in this way, the epitaxial misfit strain acts as a handle to vary the relative energies of the possible bulk phases. We have simulated coherent epitaxial (001) films of $\text{Bi}_2\text{NiMnO}_3$ by doing calculations of the bulk material where we impose mechanical boundary conditions determined by the lattice constant of the substrate, assumed to display in-plane square symmetry (this is indeed the case for many perovskite substrates cut perpendicularly to one of the principal axes).

As a starting point, we adapted the three bulk phases described in the previous section to the in-plane square symmetry. There are two inequivalent ways to do this for the GS and p phases, and one way for the R phase, as shown in Fig. 1. This causes small distortions to bring the in-plane lattice vectors to form a 90° angle and to be of the same magnitude (in the adapted p and R phases) or of a ratio of magnitudes equal to two (in the GS phase). In all cases, those distortions cost only a few meV per formula unit. Then, we do calculations in which we expand or contract the lattice vectors to mimic the effect of squared substrates with different lattice constants. We do this in intervals of 0.05 \AA , and we use the Wickoff positions and out-of-plane lattice vector of the previous geometry as a starting point of the next geometry relaxation. In this way, we arrive at a graphic of the energy of the films as a function of in-plane lattice constant that we show in Fig. 3 (top). These calculations were done using the DFT+ U method.

For strains around the minimum of the energy curves the adopted configuration is paraelectric. However, for high enough tensile strains the R phase has lower energy than the other phases. These strains correspond to in-plane lattice constants of the order of 4 \AA , so this phase is expected to appear if the films are grown over perovskite oxides such as BaTiO_3 or $\text{PbZr}_{1-x}\text{Ti}_x\text{O}_3$ (PZT). Figure 3 (bottom) shows that the computed polarization of the films is similar to the $70 \mu\text{C}/\text{cm}^2$ of the bulk phase. The electronic structure of the films is very similar to that of the bulk, as illustrated in Fig 2 for the film with in-plane lattice parameter $a = 4 \text{ \AA}$.

All GS, p , and R films at tensile epitaxial strains have magnetic cations with magnetic moments around $3\mu_B$ for Mn^{4+} and around $2\mu_B$ for Ni^{2+} . Figure 4(a) shows that below in-plane lattice parameters around 4.05 \AA ferromagnetism prevails over the alternative antiferromagnetic orderings typical of perovskites: G type (antiferromagnetism in-plane and out-of-plane), C type (ferromagnetism out-of-plane), and A type (ferromagnetism in-plane). This is not surprising, since the network of

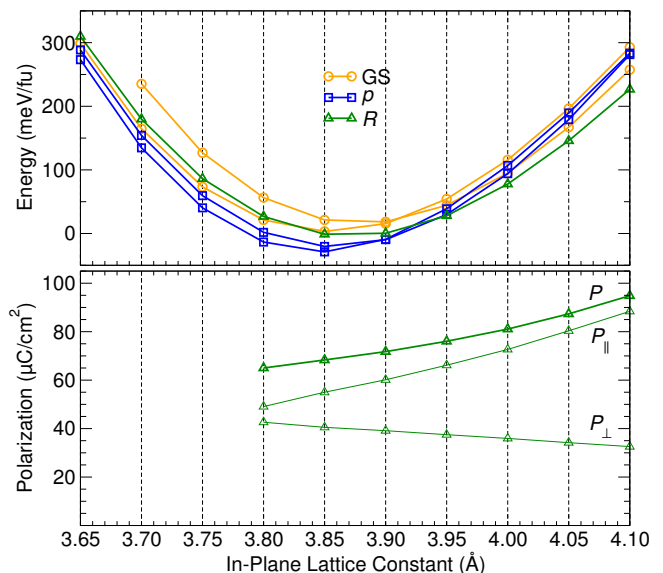


FIG. 3. (Color online.) Top: DFT+ U energy of relaxed (001) films as a function of the in-plane lattice parameter; the films are adaptations of the bulk GS (two possible orientations), p (two possible orientations), and R (one inequivalent orientation) phases to the mechanical boundary conditions imposed by the square symmetry of the substrate. Bottom: magnitude of the polarization of the R films (P), its component on the film (P_{\parallel}), and its component perpendicular to the film (P_{\perp}).

transition-metal ions and oxygens connecting them has angles and bond lengths similar to those of the bulk network, known to be ferromagnetic.

Following a prescription we have described in earlier articles,^{30,48,56} we have used the DFT+ U energy differences between magnetic arrangements to fit a simplified Heisenberg model. This model has as parameters two exchange constants J_a and J_c that take into account the strength of the magnetic interaction between neighboring Ni–Mn pairs in plane and out of plane, respectively; their values are represented in 4(b). A Monte Carlo method on a lattice of $20 \times 20 \times 20$ spins was used with this Heisenberg model to study the behaviour of the magnetic ordering with temperature. Doing this, we found that the ferromagnetic order parameter takes values other than zero for temperatures below a Curie point of around 100 K, as shown in 4(c); this is in agreement with experimental measurements done in $\text{Bi}_2\text{NiMnO}_3$ films.⁵⁰ The magnetic susceptibility computed from the Monte Carlo simulations with this Heisenberg model is plotted in Fig. 4(d).

The results for films presented so far were obtained using DFT+ U calculations. As for BiMnO_3 ,³⁰ this methodology does not resolve the close energy differences between phases in agreement with experiment, but the HSE06 hybrid functional does. When we applied it to do computations for tensile films of $\text{Bi}_2\text{NiMnO}_6$ it also predicted that the R phase is the most stable one for large enough strains, as shown in Fig. 5.

In order to further explore the energy surface of bulk

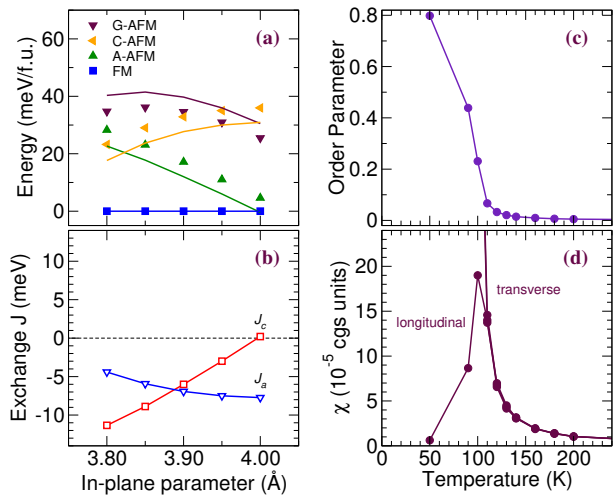


FIG. 4. (Color online.) Magnetic properties of R films: (a) DFT+ U values of the energy of different magnetic arrangements (symbols) and fit to a Heisenberg model (lines); (b) exchange coupling constants J that result from this fit; (c) ferromagnetic order parameter as a function of temperature obtained from the Heisenberg model when $a = 3.95$ Å; and (d) longitudinal and transverse magnetic susceptibility obtained from the Heisenberg model when $a = 3.95$ Å.

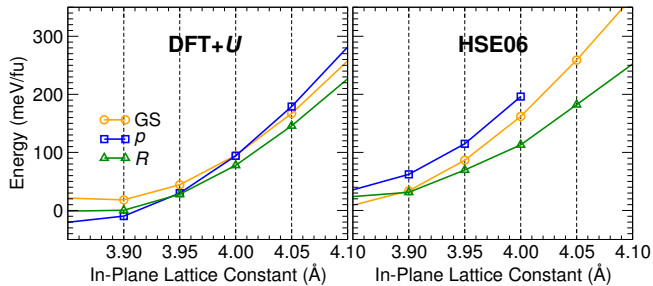


FIG. 5. (Color online.) Comparison of the energy of relaxed films as a function of the in-plane lattice parameter when using DFT+ U (left) and HSE06 (right). When two orientations of the films are possible (GS and p phases) we have done HSE06 calculations for the one with lowest DFT+ U energy in most of the range of in-plane lattice parameters.

$\text{Bi}_2\text{NiMnO}_6$ in the search of minima that might be relevant in films, we did one more set of calculations. We took every film structure represented by a point in Fig. 3, removed the epitaxial constraints, performed a few steps of molecular dynamics to allow it to explore its surroundings, and relaxed this structure until the forces and stresses were almost zero. During this annealing process the atoms visited structures that were up to a few eV/fu higher in energy than the ground state. By the end of the search, most of the initial structures had converged to a configuration with forces below 0.015 eV/Å, and these are represented in Fig. 6, where the energy with respect to the bulk ground state is plotted as a function of the average of the two closest in-plane lattice constants of the optimized structure. We see that the low-energy points

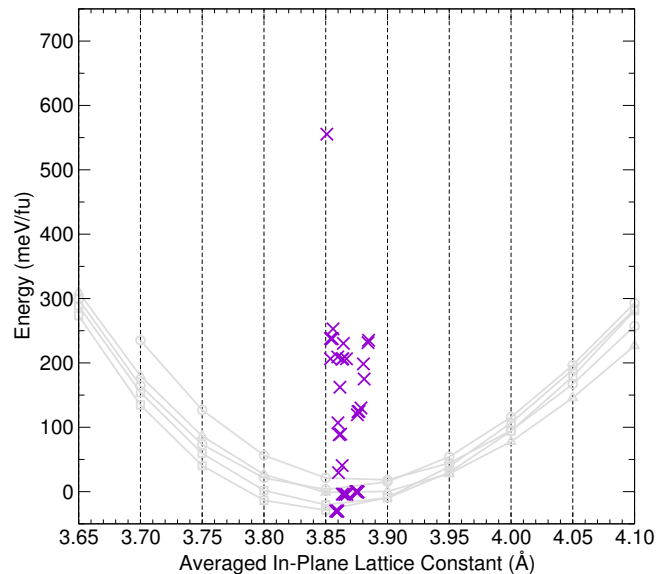


FIG. 6. (Color online.) The crosses correspond to the energy of the bulk optimized structures that result after performing an annealing on each of the film structures recorded in Fig. 3 as described in the text. In gray we have copied the data of Fig. 3 for reference.

are near the minima of the film curves of Fig. 3, showing that in several cases releasing the epitaxial constraints just takes the system to one of the three bulk phases described in this work. After analyzing the rest of the crosses in Fig. 6, it turns out that they also correspond to one of the GS, p , or R phases, but with a different electronic configuration (e.g., the value at around 550 meV/fu is a R structure where all ions show zero magnetic moments). In all, we are confident that no other low energy structures exist for typical in-plane lattice constants, and in particular in the region where the films are found to be ferroelectric and ferromagnetic.

IV. SUMMARY AND CONCLUSIONS

Our first-principles calculations for bulk $\text{Bi}_2\text{NiMnO}_6$ are consistent with a non-polar crystal structure of space group $C2/c$. Previous reports pointed out to a $C2$ polar space group, but the reasons stated in Section III.A lead us to believe that, as it happened with BiMnO_3 , this is not correct.

Our calculations also show that when $\text{Bi}_2\text{NiMnO}_6$ is grown on a (001)-oriented perovskite substrate of materials such as BaTiO_3 or PZT the epitaxial strain should favour a phase that is both ferroelectric and ferromagnetic. The polarization of these films is around 70 $\mu\text{C}/\text{cm}^2$, similar to that of the most used ferroelectric materials. The films are predicted to be ferromagnetic with magnetic moments of 2.5 μ_B per formula unit and a Curie temperature of around 100 K. Thus, our simulations predict that, in thin film form, $\text{Bi}_2\text{NiMnO}_6$ is one

of the very few known magnetoelectric multiferroics with a strong ferromagnetic order.

ACKNOWLEDGEMENTS

O.D. acknowledges funding from the Israel Science Foundation through Grants 1814/14 and 2143/14. J.Í. was financially supported by the Luxembourg National Research Fund through the Pearl (Grant No. P12/485315) and Core (Grant No. C15/MS/10458889) programs.

-
- ¹ M. Bibes and A. Barthélemy, *Nat. Mater.* **7**, 425 (2008).
² N.A. Hill, *J. Phys. Chem. B* **104**, 6694 (2000).
³ S. Bhattacharjee, E. Bousquet, and P. Ghosez, *Phys. Rev. Lett.* **102**, 117602 (2009).
⁴ M. Fiebig, *J. Phys. D: Appl. Phys.* **38**, R123 (2005).
⁵ W. Prellier, M.P. Singh, and P. Murugavel, *J. Phys.: Condens. Matter* **17**, R803 (2005).
⁶ D.I. Khomskii, *J. Magn. Magn. Mater.* **306**, 1 (2006).
⁷ W. Eerenstein, N.D. Mathur, and J.F. Scott, *Nature* **442**, 759 (2006).
⁸ C.N.R. Rao and C.R. Serrao, *J. Mater. Chem.* **17**, 4931 (2007).
⁹ R. Ramesh and N.A. Spaldin, *Nat. Mater.* **6**, 21 (2007).
¹⁰ Y. Tokura, *J. Magn. Magn. Mater.* **310**, 1145 (2007).
¹¹ S.W. Cheong and M. Mostovoy, *Nat. Mater.* **6**, 13 (2007).
¹² C.-W. Nan, M.I. Bichurin, S. Dong, D. Viehland, and G. Srinivasan, *J. Appl. Phys.* **103**, 31101 (2008).
¹³ K.F. Wang, J.-M. Liu, and Z.F. Ren, *Adv. Phys.* **58**, 321 (2009).
¹⁴ A.R. Akbashev and A.R. Kaul, *Russ. Chem. Rev.* **80**, 1159 (2011).
¹⁵ J. Ma, J. Hu, Z. Li, and C.-W. Nan, *Adv. Mater.* **23**, 1062 (2011).
¹⁶ A.P. Pyatakov and A.K. Zvezdin, *Phys.-Usp.* **55**, 557 (2012).
¹⁷ G. Catalan and J. F. Scott, *Adv. Mater.* **21**, 2463 (2009).
¹⁸ J.H. Lee, L. Fang, E. Vlahos, X. Ke, Y.W. Jung, L.F. Kourkoutis, J.-W. Kim, P.J. Ryan, T. Heeg, M. Roeckerath, V. Goian, M. Bernhagen, R. Uecker, P.C. Hammel, K.M. Rabe, S. Kamba, J. Schubert, J.W. Freeland, D.A. Muller, C.J. Fennie, P. Schiffer, V. Gopalan, E. Johnston-Halperin, and D.G. Schlom, *Nature* **466**, 954 (2010).
¹⁹ M. Angst, *Phys. Status Solidi RRL* **7**, 383 (2013).
²⁰ I.K. Yang, J. Kim, S.H. Lee, S.-W. Cheong, and Y.H. Jeong, *Appl. Phys. Lett.* **106**, 152902 (2015).
²¹ J. van den Brink and D.I. Khomskii, *J. Phys.: Condens. Matter* **20**, 434217 (2008).
²² Y. Yamasaki, S. Miyasaka, Y. Kaneko, J.-P. He, T. Arima, and Y. Tokura, *Phys. Rev. Lett.* **96**, 207204 (2006).
²³ M. Gich, I. Fina, A. Morelli, F. Sánchez, M. Alexe, J. Gàzquez, J. Fontcuberta, and A. Roig, *Adv. Mater.* **26**, 4645 (2014).
²⁴ T. Atou, H. Chiba, K. Ohoyama, Y. Yamaguchi, and Y. Syono, *J. Solid State Chem.* **145**, 639 (1999).
²⁵ A. Moreira dos Santos, A. K. Cheetham, T. Atou, Y. Syono, Y. Yamaguchi, K. Ohoyama, H. Chiba, and C. N. R. Rao, *Phys. Rev. B* **66**, 064425 (2002).
²⁶ A. A. Belik, S. Iikubo, T. Yokosawa, K. Kodama, N. Igawa, M. Azuma, M. Takano, K. Kimoto, Y. Matsui, and E. Takayama-Muromachi, *J. Am. Chem. Soc.* **129**, 971 (2007).
²⁷ E. Montanari, G. Calestani, L. Righi, E. Gilioli, F. Bolzoni, K.S. Knight, and P.G. Radaelli, *Phys. Rev. B* **75**, 220101 (2007).
²⁸ P. Baettig, R. Seshadri, and N.A. Spaldin, *J. Am. Chem. Soc.* **129**, 9854 (2007).
²⁹ A. J. Hatt and N. A. Spaldin, *Eur. Phys. J. B* **71**, 435 (2009).
³⁰ O. Diéguez and J. Íñiguez, *Phys. Rev. B* **91**, 184113 (2015).
³¹ J.B. Goodenough, *J. Phys. Chem. Solids* **6**, 287 (1958).
³² J. Kanamori, *J. Phys. Chem. Solids* **10**, 87 (1959).
³³ M. Azuma, K. Takata, T. Saito, S. Ishiwata, Y. Shimakawa, and M. Takano, *J. Am. Chem. Soc.* **127**, 8889 (2005).
³⁴ A. Ciucivara, B. Sahu, and L. Kleinman, *Phys. Rev. B* **76**, 064412 (2007).
³⁵ H.J. Zhao, X.Q. Liu, and X.M. Chen, *AIP Advances* **2**, 22115 (2012).
³⁶ H.J. Zhao and X.M. Chen, *AIP Advances* **2**, 42143 (2012).
³⁷ P. Hohenberg and W. Kohn, *Phys. Rev.* **136**, B864 (1964).
³⁸ W. Kohn and L. J. Sham, *Phys. Rev.* **140**, A1133 (1965).
³⁹ A. I. Liechtenstein, V. I. Anisimov and J. Zaanen, *Phys. Rev. B* **52**, R5467 (1995).
⁴⁰ A. V. Krukau, O. A. Vydrov, A. F. Izmaylov, and G. E. Scuseria, *J. Chem. Phys.* **125**, 224106 (2006).
⁴¹ G. Kresse and J. Furthmüller, *Phys. Rev. B* **54**, 11169 (1996); G. Kresse and D. Joubert, *Phys. Rev. B* **59**, 1758 (1999).
⁴² A. Stroppa and S. Picozzi, *Phys. Chem. Chem. Phys.* **12**, 5405 (2010).
⁴³ J.P. Perdew, A. Ruzsinszky, G.I. Csonka, O.A. Vydrov, G.E. Scuseria, L.A. Constantin, X. Zhou, and K. Burke, *Phys. Rev. Lett.* **100**, 136406 (2008).
⁴⁴ P. E. Blöchl, *Phys. Rev. B* **50**, 17953 (1994).
⁴⁵ K. Takata, M. Azuma, Y. Shimakawa, and M. Takano, *J. Jap. Soc. Powder Powder Metallurgy* **52**, 913 (2005).
⁴⁶ A.A. Belik, *J. Solid State Chem.* **195**, 32 (2012).
⁴⁷ O. Diéguez, O.E. González-Vázquez, J.C. Wojdél, and J. Íñiguez, *Phys. Rev. B* **83**, 094105 (2011).
⁴⁸ O. Diéguez and J. Íñiguez, *Phys. Rev. Lett.* **107**, 057601 (2011).
⁴⁹ Y. Uratani, T. Shishidou, F. Ishii, and T. Oguchi, *Physica B* **383**, 9 (2006).
⁵⁰ M. Sakai, A. Masuno, D. Kan, M. Hashisaka, K. Takata, M. Azuma, M. Takano, and Y. Shimakawa, *Appl. Phys. Lett.* **90**, 72903 (2007).
⁵¹ Y. Shimakawa, D. Kan, M. Kawai, M. Sakai, S. Inoue, M. Azuma, S. Kimura, and O. Sakata, *Jpn. J. Appl. Phys.* **46**, L845 (2007).
⁵² J.L. Lai, X.G. Tang, C.B. Ma, R. Li, Q.X. Liu, and

- Y.P. Jiang, *Integrated Ferroelectrics* **139**, 26 (2012).
- ⁵³ H. Jeon, G. Singh-Bhalla, P. R. Mickel, K. Voigt, C. Morien, S. Tongay, A. F. Hebard, and A. Biswas, *J. Appl. Phys.* **109**, 074104 (2011).
- ⁵⁴ J.Y. Son and Y.-H. Shin, *Appl. Phys. Lett.* **93**, 062902 (2008).
- ⁵⁵ G.M. De Luca, D. Preziosi, F. Chiarella, R.D. Capua, S. Gariglio, S. Lettieri, and M. Salluzzo, *Appl. Phys. Lett.* **103**, 062902 (2013).
- ⁵⁶ C. Escorihuela-Sayalero, O. Diéguez, and J. Íñiguez, *Phys. Rev. Lett.* **109**, 247202 (2012).